Journal of Fluorine Chemistry 134 (2012) 90–102

Contents lists available at ScienceDirect

Journal of Fluorine Chemistry

journal homepage: www.elsevier.com/locate/fluor

Strasbourg's SOFFT team—Soft functional systems self-assembled from perfluoroalkylated molecular components

Marie Pierre Krafft *

Systèmes Organisés Fluorés à Finalités Thérapeutiques (SOFFT), Institut Charles Sadron (CNRS UPR 22), Université de Strasbourg, 23 rue du Loess, 67034 Strasbourg Cedex 2, France

ARTICLE INFO

Article history:
Received 18 January 2011
Received in revised form 11 April 2011
Accepted 14 April 2011
Available online 22 April 2011

Keywords:
Fluorosurfactant
Fluorous
Surface micelle
Emulsion
Microbubble

ABSTRACT

The SOFFT (Systèmes Organisés Fluorés Fonctionnels à Finalités Thérapeutiques) team is engaged in the design, building, characterization and assessment of highly fluorinated functional self-assembled molecular systems (*F*-SAMS, i.e. fluorinated soft matter). Therefore, it synthesizes dedicated fluorinated building blocks and exploits the specific properties of highly fluorinated chains and components ("hyper"hydrophobicity, lipophobicity, volume, rigidity, surface properties, etc.) to drive self-assembly. The systems investigated include interfacial films and membranes, 2D arrays of surface micelles, composite multilayered films, fluorinated vesicles and tubules, diverse types of emulsions, microbubbles and decorated microbubbles, for which preparation and characterization techniques have been developed. Fluorinated components are used to modify and control phospholipid film and membrane behavior, stabilize and control emulsion and microbubble characteristics, generate micro- and nanocompartments, useful as templates for polymerization or for confinement. Key findings include formation on water and solid supports of surface hemimicelles that provide nanometer-size surface patterns; stacking of self-assembled hemimicelles; reversible vertical phase segregation in surface films; exploration of 2D/3D transitions in surface films; obtaining of facetted fluid vesicles; improved emulsion and bubble stabilization and particle control; determination of the mechanism of emulsion stabilization by (*F*-alkyl)alkyl diblocks; characterization of a co-surfactant effect for non-polar molecules; obtaining of narrowly sized populations of stable microbubbles; and correlation of bubble size and stability with wall and internal phase components. Targeted applications include lung surfactant replacement preparations; adhesion control of cells capable of insulin production; parenteral oxygen delivery and pulmonary drug delivery; and tools for biomedical research. Multiscale objects are currently being investigated, such as microbubbles decorated with magnetic particles destined for multimodal diagnostic imaging and, in materials science, for their non-linear magnetic, optical and magneto-optic properties.

1. Introduction

This paper is part of a Special Issue of the Journal that focuses on Fluorine Chemistry in France. It highlights some recent results of the SOFFT team (Systèmes Organisés Fluorés à Finalités Thérapeutiques) at the University of Strasbourg (see "Research topics" at the end of the paper).

2. Synthesis of small highly fluorinated amphiphilic molecules

The research effort of the SOFFT team is organized as depicted in Scheme 1.

A notable strategic advantage of the team is that it has developed a capacity for tailor-synthesizing the molecular fluorinated components (or building blocks) that it needs for building the systems it selects to investigate. These components generally consist of amphiphilic molecules that comprise one or more perfluoroalkylated chains (*F*-chains)[1] [1]. Typical examples of such compounds include the (*F*-alkyl)alkyl diblocks $C_nF_{2n+1}C_mH_{2m+1}$ (*FnHm*) **1**, (alkyl)*F*-alkyl(alkyl) triblocks $C_mH_{2m+1}C_nF_{2n}C_mH_{2m+1}$ (*HmFnHm*) **2**, *F*-alkylated phosphocholines $C_nF_{2n+1}C_mH_{2m}OP(O)_2^-OCH_2CH_2N^+Me_3$ (*FnHm*PC) **3**, *F*-alkylated phosphatidylcholines $C_nF_{2n+1}C_mH_{2m}C(O)\ OCH_2[C_nF_{2n+1}C_mH_{2m}C(O)O]CHCH_2OP(O)_2^-OCH_2CH_2NMe_3^+$ (di(*FnHm*)GPC) **4**, single and double-chain *F*-alkylphosphates (*FnHm*Phos) **5** and (di(*FnHm*)GPhos) **6**, *F*-alkyl mono- and dimorpholinophosphates

[1] Now commonly used, the *italized*, *F*- (for perfluoro or perfluorinated) short notation will be used throughout this paper to designate perfluoroalkyl (*F*-alkyl) moieties and, by extension, constructs (e.g. *F*-vesicles) made from *F*-alkylated components [1]. The *H*-notation will designate their hydrocarbon counterparts (e.g. *H*-alkyl, *H*-vesicles). Fluorocarbons and hydrocarbons will be denoted *FC* and *HC*, respectively.

* Tel.: +33 3 88 41 40 60; fax: +33 3 88 40 41 99.
E-mail address: krafft@ics.u-strasbg.fr.

0022-1139/$ – see front matter © 2011 Elsevier B.V. All rights reserved.
doi:10.1016/j.jfluchem.2011.04.009

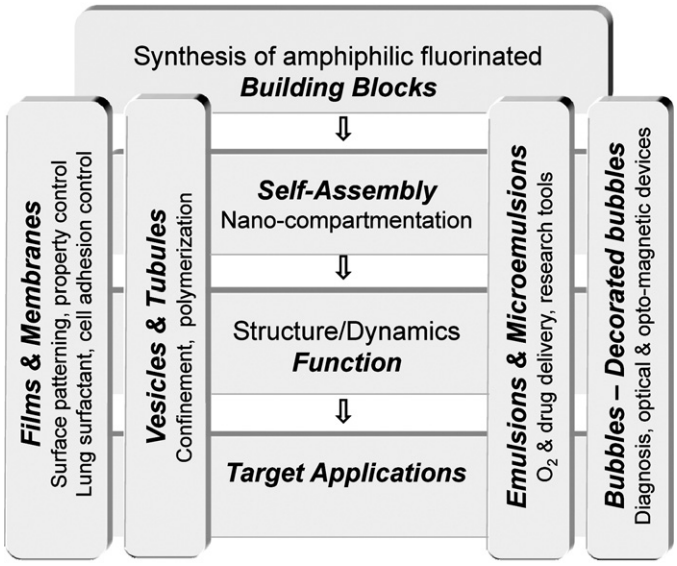

Scheme 1. Schematic overview of SOFFT's approach to fluorinated self-assembled molecular systems (*F*-SAMS).

$(C_nF_{2n+1}C_mH_{2m}O)_{1\ or\ 2}P(O)[N(CH_2CH_2)_2O]_{2\ or\ 1}$ (*FnHm*DMP) **7** and (di(*FnHm*)MMP) **8**, pegylated amphiphiles (*FnHm*PEG) **9**, aminoxides $C_7F_{15}C(O)NH(CH_2)_3N(O)(CH_3)_2$ **10**, "reverse" semifluorinated amphiphiles $C_mH_{2m+1}C_nF_{2n}OP(O)[N(CH_2CH_2)_2O]_2$ (*HmFn*DMP) **11**, catanionic octyltrimethylammonium *F*-octanoate $C_7F_{15}COO^-\ C_8H_{17}N^+(CH_3)_3$ **12** and, among our more recently synthesized amphiphiles, the novel star-shaped polyphilic compounds **13** and non-polar "gemini" tetrablocks **14**. These compounds cover a wide range of lengths, polar head sizes, hence packing parameters (in the sense of Israelachvili) [2], surface activities, hydrophilic/hydrophobic balances, etc.

Many of the constructs we investigate take advantage of the unique properties of the simple *FnHm* diblocks **1** (Turberg and Brady's "primitive" surfactants [3]), which proved exceptionally useful as building blocks for self-assembled *F*-constructs and as tools for film behavior control. *FnHm* diblocks, although they are devoid of polar head, are nevertheless amphiphilic, amphisteric, and amphidynamic [1].

The usually straightforward synthetic approaches used for preparing some recently reported compounds are exemplified below and depicted in Scheme 2.

2.1. Star-shaped "schizophrenic" triphilic amphiphiles

Compounds **13** (Scheme 2a) comprise three arms that have antagonistic affinities, a fluorinated chain (hydrophobic and lipophobic), a hydrocarbon chain (hydrophobic and fluorophobic) and a methyl-caped poly(ethylene glycol) (PEG) chain (hydrophilic) that are interconnected in a Y arrangement via a double bond. These compounds were needed to explore new ways of achieving nanocompartmentation in self-assemblies. Their synthesis involved 3-*F*-alkyloxypropanoic acids, **15**, as the key intermediates, on which the PEG chains were subsequently grafted [4]. Use of monodisperse methyl-caped di- and triethylene glycols led to the corresponding triaffine surfactants. Alternately, a library of five triaffine compounds was obtained from polydisperse MPEG 350 (a mixture of oligomers) from which the pure individual triaffines were separated by column chromatography. The *Z* isomer was largely predominant and most compounds were isolated in isomerically pure form.

2.2. Gemini tetrablock amphiphiles

The "non-polar" fluorophilic/lipophilic amphiphilic tetrablocks **14** (di(*FnHm*)), Scheme 2b, comprise two lipophobic fluorinated and two fluorophobic hydrogenated blocks and no hydrophilic moiety. The flexibility of the central six-carbon linking unit facilitates conformational adjustments as needed for self-assembly. Such compounds were required for advancing our understanding of surface film patterning and hemimicelle formation from non-hydrophilic molecules, and for the exploration of 2D/3D transitions in such films. Their two-step synthesis of di(*FnHm*) tetrablocks involved radical addition of an *F*-alkyl iodide to a linear terminal alkene, followed by a Wurtz-type coupling of two molecules of the resulting adduct, **16**, using activated zinc nanopowder [5]. The threo isomer was formed exclusively when $n = 10$; for $n = 8$, the shorter the *Hm* block, the larger was the amount of erythro diastereoisomer formed.

2.3. Sequential triphilic amphiphiles

Various amphiphiles combining fluorophilic, lipophilic and hydrophilic moieties in linear sequences were prepared. The single-chain (*F*-alkyl)alkylphosphates **5** were obtained through phosphorus oxychloride phosphorylation of the appropriate alcohols, followed by hydrolysis. Aminolysis with morpholine provided the phosphomorpholidates **7** and **8** that proved highly effective for tubule generation, stabilization of reverse water-in-*F*C emulsions, and basic research [6,7]. Two double chain (*F*-alkyl)alkylglycerophosphates **6** (Scheme 2c) were prepared in ~40% yield by phosphorylation of *rac*-1,2-di-(*F*-alkylacyl)-3-glycerols using $POCl_3$, followed by hydrolysis (~50% yield). The intermediate 1,2-disubstituted glycerols, **17** (Scheme 2c), resulted (>85% yield) from acylation of *rac*-1-benzyl-glycerol with the appropriate *F*-alkanoyl halides. The protecting benzyl group was removed by hydrogenation on a Pd/C catalyzer.

The pegylated compounds **9** (Scheme 2d) that are potentially capable of conferring some "stealthiness" to particles in vivo, were isolated (~70% yield) from the reaction of (*F*-alkyl)alkanoic chlorides on poly(oxyethylene)glycol monomethylethers.

Access to the "reverse" (alkyl)*F*-alkyl amphiphiles **11** (Scheme 2e), which display an inner *F*-alkyl segment, and are useful for assessing the role of the position *F*-chains, terminal or not, in self-assembly, required the synthesis of dissymmetric ω-functionalized *F*-alkyl iodide precursors. The methyl 9-iodo-*F*-nonanoate intermediate **18** was prepared from dimethyl *F*-sebacate **19** obtained from *F*-sebacic acid and diazomethane in ether [8]. Subsequent partial hydrolysis, treatment with silver nitrate, followed by a Hunsdieker-type reaction with iodine, yielded the expected ω-functionalized *F*-alkyl iodide. Radical addition of **19** to 1-decene and dehalogenation of the adduct with tributyltin hydride in the presence of azobis(isobutyronitrile) (AIBN) yielded **20**. Reduction of the latter to the alcohol, followed by a one-pot treatment with phosphorus oxychloride and morpholine led to the desired "reverse" surfactants **11**. The *HmFnHm* triblocks **2** (Scheme 2f), also with an internal *F*-segment resulted from the classical radical addition of two alkenes on an α,ω-*F*-alkyl diiodide.

3. Preparation of fluorinated self-assembled molecular systems

The central undertaking of the SOFFT team is to design, build and investigate highly fluorinated self-assembled molecular systems (*F*-SAMS). These systems include complex 2-dimensional self-assembled films and membranes, usually formed at interfaces, and 3-dimensional discrete objects, such as vesicles, tubules,

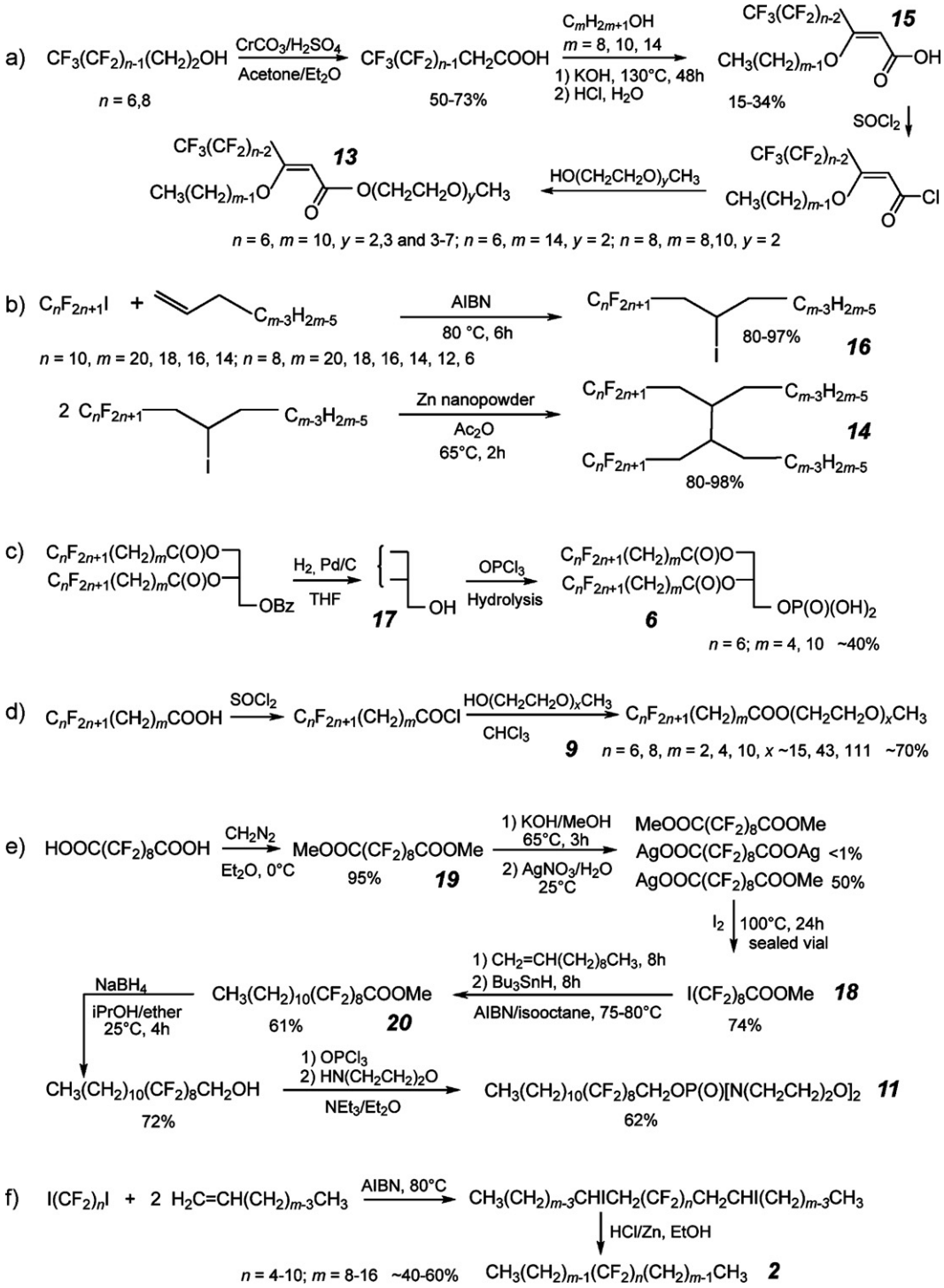

Scheme 2. Synthesis of some recently reported fluorinated amphiphilic building blocks.

emulsions and microbubbles (Scheme 3). Our approach to *F*-SAMS relies primarily on the powerful capacity for *F*-chains to promote self-assembly and depends on the "superhydrophobicity"-driven affinity of *F*-alkyl chains for *F*-alkyl chains, which was also the basis for separation of *F*-alkylated compounds on *F*-alkylated silica [9]. The same effect is also being implemented in "fluorous" chemistry [10]. Our systems take into account some specific constraints prescribed by biomedical target applications [11–13] and belong to the realm of, and benefit from the investigation techniques relevant to soft matter.

3.1. Two-dimensional self-assemblies—films and membranes

We prepare surface films and interfacial films of *F*-amphiphiles or of mixtures of *F*-amphiphiles with other amphiphiles, mostly phospholipids, using the Langmuir trough or pending or rising dynamic tensiometry bubble or drop methodologies. Such films are also deposited on solid surfaces using Langmuir–Blodgett and spin-coating techniques.

Special attention is being devoted to the nano-patterned films that result from the spontaneous self-assembly on water and on

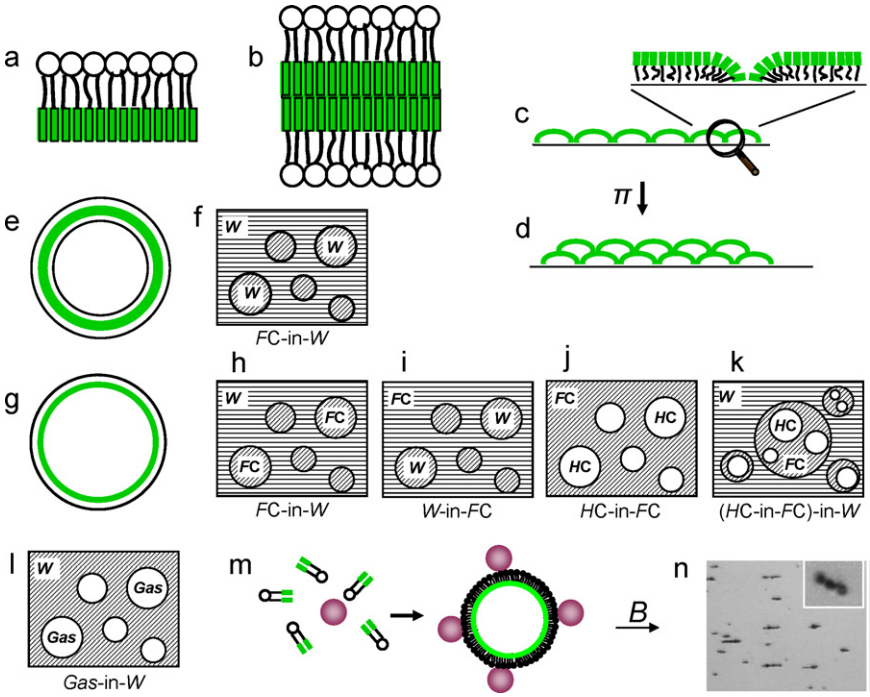

Scheme 3. Schematic representation of the 2D and 3D *F*-systems investigated (*F*-sub-layers in green); (a) and (b) monolayer and bilayer made from *F*-amphiphiles; (c) and (d) monolayer and stacked layers of self-assembled surface hemimicelles of *FnHm* diblocks; (e) *F*-vesicle, (f) the same dispersed in water; (g) microdroplet or microbubble with *F*-wall components; (h–k) various types of emulsions (the *F*-layer is outside the droplets in (j), inside or outside in (k)); (l) gas emulsion (bubble dispersion); (m) self-assembly of multi-scale nanoparticle-decorated microbubbles (NP-*deco*MBs); (n) Fe_3O_4NP-*deco*MBs align in a magnetic field. (For interpretation of the references to color in this figure legend, the reader is referred to the web version of this article.)

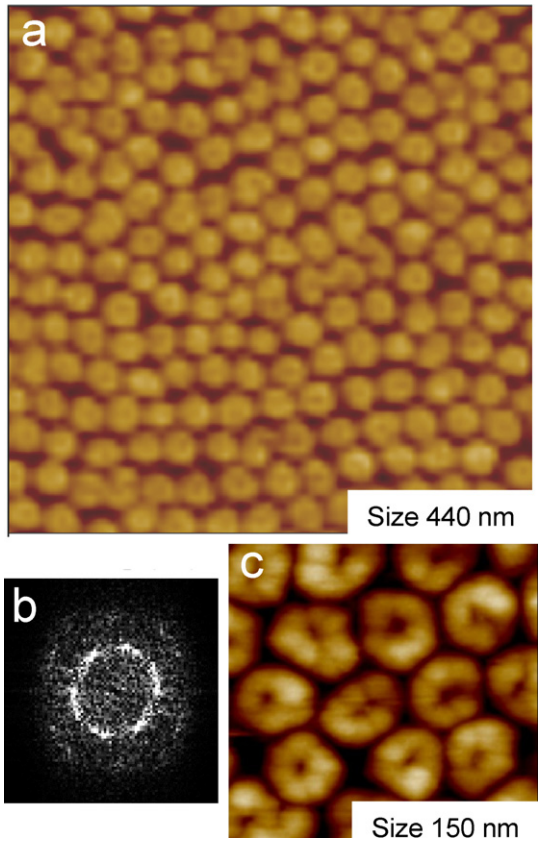

Fig. 1. AFM image (tapping mode, topography, 440 nm × 440 nm) of a Langmuir monolayer of *F8H*16 transferred on a silicon wafer by a Langmuir–Blodgett procedure at a pressure of 7 mN m^{-1} [37], (b) two-dimensional Fourier transform of (a) showing two rings; (c) typical hexagonal network of hemimicelles (150 nm × 150 nm; transfer pressure: 6 mN m^{-1}).

solid surfaces of *hemimicelles* of *FnHm* diblocks **1** (Fig. 1) and di(*FnHm*) tetrablocks **14** (Section 3.1). Exploration of the isothermal compression of Langmuir films of diblocks and tetrablocks *beyond* the film collapse documented in the literature led to complex multilayer arrangements as well as to *stacked* self-assembled nano-objects (Section 3.2).

Mixed films were investigated in relation with control of phospholipid film behavior, cell adhesion studies, and lung surfactant replacement preparations [14–17].

3.2. Discrete three-dimensional micro- and nanometer size two-phase self-assembled objects—fluorinated vesicles and tubules

3.2.1. Fluorinated vesicles

Several approaches have been devised that allowed us to prepare *F*-vesicles and *F*-tubules. They include self-assembly of single chain partially *F*-alkylated phosphocholines **3** or double-chain *F*-alkylated phospholipids **4** or glucophospholipids (6-glucose-$P(O)_2^-OCH(C_9H_{19})C_2H_4C_8F_{17}$) [18]; combinations of *FnHm* diblocks **1** or *HmFnHm* triblocks "tie-bars" **2** with standard non-fluorinated phospholipids; association of *F*-alkylated single-chain amphiphiles (e.g. **3**) with *FnHm* diblocks "crutches" **1**. In all cases, substantial stabilization was noted relative to related standard non-fluorinated vesicles.

3.2.2. Faceted vesicles

We recently obtained polyhedral vesicles using the catanionic amphiphile octyltrimethylammonium *F*-octanoate **12** ($C_7F_{15}COO^-$ $C_8H_{17}N^+(CH_3)_3$, a perfluorinated anion associated with a hydrogenated cation) as wall component. The initially formed vesicles are spherical (Fig. 2a). They spontaneously turn into faceted vesicles within a few weeks at room temperature (Fig. 2b) [19]. Contrary to the previously reported faceted vesicles, whose membrane is in the gel state [20,21], the membrane of those made from **12** remains in the fluid state, providing the first known example of fluid faceted

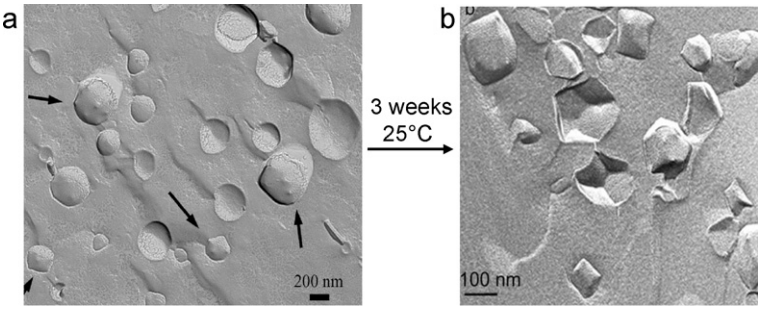

Fig. 2. Freeze-fracture transmission electronic microscopy of vesicles self-assembled from the catanionic amphiphile **12** (a) 1 week after preparation; (b) after 1 month at 25 °C [19].

vesicles. Facet formation was attributed to partial segregation of the fluorinated anions from the non-fluorinated cations within the bilayer membrane.

3.2.3. Tubules

The first tubules made by spontaneous self-association of non-chiral molecular components and in the absence of hydrogen bonds were obtained from dimorpholinophosphate **7** ($n = 8$, $m = 2$) [22,23]. pH-sensitive tubules were obtained from *F*-alkylated glucophospholipids [24,25]. At high pH, formation of hydrogen bonds promotes in this case tubule formation, while at low pH, vesicles are favored. The mechanism of tubule formation has been unraveled. Reversible tubule/vesicle interconversion was demonstrated [26] (collaboration with T. Imae, Nagoya University). The self-assembly behavior of *F*-amphiphiles, also in combination with *F*-alcohols [27], has been investigated in water, aqueous buffers, and organic solvents [28].

3.3. Discrete three-dimensional, three-phase micro- and nanometer-size self-assembled objects—emulsions and microbubbles

Three phases (i.e. *F*C, water or gas, and an interfacial film of a surfactant or surfactant mixture) or more were combined to form emulsions and microbubbles (gas emulsions) (Scheme 3). The analogy of *F*Cs and gases from the standpoint of their low intermolecular cohesion forces is well known.

3.3.1. Fluorocarbon-in-water emulsions

We have devised procedures that allow preparation of *F*C-in-water emulsions specifically tailored for the study of stabilization mechanisms, particle size control, or particular applications. These emulsions are generally formulated with phospholipids as the emulsifier, usually supplemented by stabilization additives according to various stabilization principles. The emulsions' concentration, droplet sizes, and other characteristics are adjusted depending on use [29], and are optionally complemented with nutrients or active components. Emulsification is achieved using high pressure/high shear microfluidization or Gaulin-type devices under nitrogen in a clean room (Fig. 3). The emulsions undergo terminal heat sterilization. Particle size measurements are performed using centrifugal photosedimentation and static or dynamic light scattering.

3.3.2. Water-in-fluorocarbon reverse emulsions

Stable "reverse" water-in-*F*C emulsions, miniemulsions and microemulsions (Scheme 3), useful as confinement domains and as vehicles for pulmonary drug delivery (Sections 4.5 and 4.6), were obtained using (*F*-alkyl)alkyldimorpholinophosphates **7** as the emulsifier and appropriate energy input, whether hand-shaking, sonication or microfluidization, depending on components and desired particle sizes [30,31]. *F*8*H*11DMP, one of the most

Fig. 3. C. de Gracia-Lux operating a high-pressure microfluidizer for fluorocarbon emulsion preparation.

biocompatible surfactant of the series, allows preparation of a wide range of stable miniemulsions (30–100 nm in droplet diameter) that can host about 5% w/v of water. Microemulsions, that is spontaneously formed, stable, small-sized dispersions (~12 nm) were also produced [31].

3.3.3. Other emulsions

Further types of emulsions, including *H*C-in-*F*C emulsions (Scheme 3) that can serve for confinement, possibly for polymerization of lipophilic monomers, were prepared using a *FnHm* diblock as the sole emulsifier. Multiple emulsions (e.g. (*H*C-in-*F*C)-in-water) were obtained through appropriate re-emulsifying sequences. Stable gel emulsions with very high internal ratios of *F*C in water (up to 98% v/v) have also been produced [32].

3.3.4. Microbubbles

Technology was established for reproducibly producing the narrowly dispersed monomodal populations of soft-shell microbubbles required for physico-chemical investigation [33]. We prepare such populations in the 1–5 μm size range using centrifugal or flotation-based fractionation following sonication of phospholipid-based compositions under an atmosphere of the filing gas mixture (usually *F*-hexane-saturated nitrogen).

Intravascular use for diagnosis or O_2 delivery requires bubble sizes lower than ~5 μm, narrow size distributions, and prolonged intravascular half-life. Other desirable features include control over bubble/ultrasound interaction and generation of harmonics.

Dedicated multifrequency experimental devices have been built that allow us to determine bubble response to ultrasound excitation both in sound transmission (acoustical determination of bubble sizes and half-lives) and in sound diffraction (capacity for generating harmonic sound waves) modes (Fig. 4) [33].

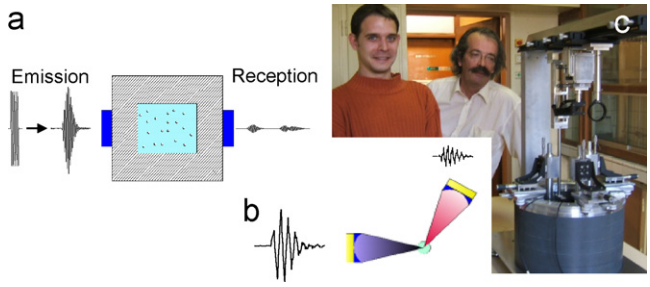

Fig. 4. Dedicated multi-frequency acoustical measurement devices and their authors, F. Gerber and G. Waton. (a) Sample cell for measurement of the attenuation coefficient of an ultrasound wave that propagates through the dispersion of microbubbles, allowing determination of their mean size and size distributions; (b) the diffracted sound signal can be detected at various angles, allowing also the instrument (c) to provide information on harmonic wave generation.

3.3.5. "Decorated" microbubbles

Microbubbles (MBs) "decorated" with magnetic iron oxide nanoparticles (NPs), yielding NP-decorated MBs (NP-*deco*MBs), are currently being prepared by forming MBs from *F*-amphiphiles fitted with a head group that allows subsequent grafting of Fe_3O_4NPs (producing Fe_3O_4NP-*deco*MBs) (Scheme 3m; collaboration with G. Pourroy et al., IPCMS Strasbourg). The amphiphile's *F*-alkyl chains and an internal *F*C gas ensure their stability (Section 4.8). Such constructs could serve as bimodal contrast agents for both ultrasound and magnetic resonance imaging.

4. Structural, dynamic and functional characteristics of fluorinated self-assembled films and objects

The above described highly fluorinated constructs are being investigated in order to determine and understand their structure, mechanism of formation, identify the features that differentiate them from non-fluorinated analogues and the role of the *F*-moieties in their formation and behavior, and explore potential functional applications. Therefore, we implement techniques commonly used for soft matter and thin film investigation both on water and on solid surfaces, including optical, Brewster angle (BAM), fluorescence and confocal microscopies; cryogenic (cryo-TEM) and freeze-fracture (FF-TEM) transmission electron microscopies; atomic force (AFM) microscopy; X-ray reflectivity, grazing incidence small-angle X-ray scattering (GISAXS); static and dynamic light scattering; differential scanning calorimetry (DSC), etc.

4.1. Highly organized arrays of surface hemimicelles of (F-alkyl)alkyl diblocks—surface nanopatterning

One of our major research topic deals with fluorinated surface films, including of the simple *FnHm* diblocks. It had been known that *FnHm* diblocks were able to form stable Langmuir monolayers [34]. Numerous studies were devoted to determining their structure [1,35,36]. The conclusions of these studies all implied the formation of continuous surface films.

An unexpected discovery was that the "non-polar" *F*8*H*16 diblock molecule, when spread on water and transferred onto a solid surface, forms regular arrays of discrete self-assembled nanometer-size domains (or *surface hemimicelles*), about 30 nm in diameter (Fig. 1) [37], rather than the expected homogeneous continuous films. The height of the domains (~3 nm) corresponds to the length of one single extended diblock molecule.

The question of the *orientation* of the diblocks was solved using X-ray reflectivity measurements, which determined that the *F*-chains were pointing upwards, while the *H*-chains were in contact with the surface of water [37]. Subsequent studies indicated that the phenomenon was general. All the diblocks investigated (**1**, $n = 8, 10$; $m = 14, 16, 18, 20$), when transferred from Langmuir films or directly deposited on silicon wafers by spin-coating, consist of discrete domains, although there are variations in their shape [38,39]. The size of the domains can be controlled by varying the length of the *Hm* block. A model was developed that accounts for this dependence [39]. Independent studies established the formation of similar self-assembled surface patterns with other diblocks, supports and deposition conditions [40,41].

A key question was whether or not self-assembly occurred directly *on the surface of water* or if it was induced by the transfer procedure or resulted from some interaction with the solid substrate after transfer. The presence of hemimicelles on the surface of water was probed using GISAXS experiments on a *F*8*H*16 monolayer directly on water (collaboration with M. Goldman et al., Europ. Synchrotron Radiation Facility, Grenoble) [42]. The study revealed a highly ordered close-packed hexagonal network, as illustrated by a 12 peak diffraction pattern. The number of peaks recorded is exceptional for a soft matter film (ESRF SpotLight on Science). Peak indexation determined the presence of large monodisperse circular domains, 33.5 nm in diameter (i.e. very close to the diameter measured by AFM on transferred monolayers). These domains form a highly organized hexagonal lattice that constitutes an almost perfect *2-dimensional crystal*. These experiments established unambiguously that self-assembly of *F*8*H*16 occurs directly on the surface of water. Ongoing studies with a range of *F*8*Hm* diblocks (**1**, $m = 14, 16, 18, 20$) confirm that formation of discrete surface domains when spread on water is a general property of *FnHm* diblocks.

Investigation of the mechanism of self-assembly for a series of *F*8*Hm* diblocks (**1**, $m = 14, 16, 18, 20$) established that hemimicelle formation depends on a critical diblock surface concentration and that the diameter of the domains is primarily controlled by the diblock's *H*-chain length. Remarkably, it is independent of surface film compression conditions [43].

Theoretical calculations based on statistical physics confirmed that *F*8*H*16 should self-assemble into stable monodisperse circular surface micelles that would organize into a hexagonal array on the surface of water [44]. The dipole moment of the CF_2–CH_2 link located between the two blocks was shown to play a key role in surface micelle formation.

Spontaneous formation of self-assembled surface domains about 40 nm in diameter and 4 nm in height was also found for the di(*F*8*H*20) tetrablock **14** [5]. Surface micelle formation was also observed with phosphates **5** and reverse surfactants **11**.

4.2. Stacking of self-assembled films and nano-objects—exploring 2D/3D transitions in nano-structured surface films

The finding of surface micelle formation from *FnHm* diblocks led us to revisit the compression behavior of Langmuir monolayers of such diblocks, and uncovered more complex behavior than previously reported [45]. A first notable feature is that the surface micelles of *FnHm* do not shrink or fuse upon compression. Exploration of Langmuir surface pressure versus molecular area isotherms *beyond* the published "collapse" pressure of monolayers of *FnHm* diblocks recently found that there actually exist an extended plateau beyond that initial "collapse" and that this plateau is followed by a *second rise* in surface pressure (Fig. 5) [45]. BAM and AFM showed that the plateau corresponds to the progressive development of a *bilayer* of diblocks on top of the initial carpet of hemimicelles. The latter are preserved throughout compression, including at the highest reachable pressures.

Compression of Langmuir films of di(*FnHm*) tetrablocks **14** takes a different turn. The compression isotherms also show a first pressure rise and, beyond the initial "collapse", a coexistence

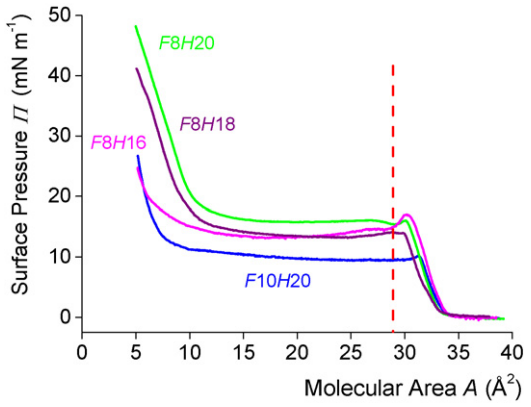

Fig. 5. Revisiting the compression isotherms of Langmuir monolayers of a series of *FnHm* diblocks deposited at the air/water interface (15 °C); on the right of the doted line are the isotherms published in the literature; on the new coexistence plateau, a double layer of diblocks develops that progressively covers the initially formed lower carpet of hemimicelles [45].

plateau that is also followed by a second pressure rise. However, instead of a continuous bilayer of diblocks (resulting in a threefold increase in film thickness), BAM and AFM established that it is a single layer of *discrete* surface micelles, essentially identical to those of the initial carpet of micelles, that develops (with a *two*fold increase in film thickness). The AFM images show the two superimposed stories of surface micelles. This appears to be the first reported example of *stacking of self-assembled nano-objects* in a surface film [5].

4.3. Fluorocarbon/hydrocarbon diblock-induced, pressure-controlled phospholipid film dynamics

Investigation of the interplay between phospholipids and *FnHm* diblocks in monolayer films and membranes was motivated by emulsion film stabilization studies and by the design of lung surfactant replacement compositions. It led to several findings, among which a new type of pressure-induced *vertical phase separation* phenomenon in which pressure causes the diblock molecules to be *reversibly* expelled from an initial mixed phospholipid plus diblock monolayer, and to organize as hemimicelles on top of a phospholipid-only monolayer [46].

Compression of a mixed monolayer of DPPE and *F8H16* was investigated on the surface of water by SAXS and AFM after transfer of the monolayer onto silicon wafers at various surface pressures [46]. At low surface pressures π, the AFM images show lateral phase separation between domains of surface micelles of diblock and of a monolayer of DPPE (Fig. 6a). As π increases, hemimicelles start to be ejected from the surface of water and the presence of higher and lower areas are seen (Fig. 6b). Further pressure increase causes the network of ejected surface micelles to start gliding on top of the DPPE monolayer, progressively overlying it, until full coverage is achieved (Fig. 6c). These micelles are essentially identical to those seen when *F8H16* is deposited alone on water and transferred on a silicon wafer (Fig. 1).

X-ray reflectivity measurements confirmed that film thickness increases with π until its height corresponds to the sum of those of a DPPE monolayer and of a layer of surface micelles of *F8H16*. Both lateral and vertical phase separation phenomena are fully *reversible*. Grazing incidence X-ray diffraction patterns recorded at low surface pressure (collaboration with M. Goldman et al., ESRF, Grenoble) confirmed complete expulsion of the diblock at high pressure, and indicated ordered arrangement of the *F*-blocks on top of the DPPE monolayer. Depending on DPPE/*F8H16* ratio, a monolayer or a bilayer of diblock was formed on top of a monolayer of the lipid.

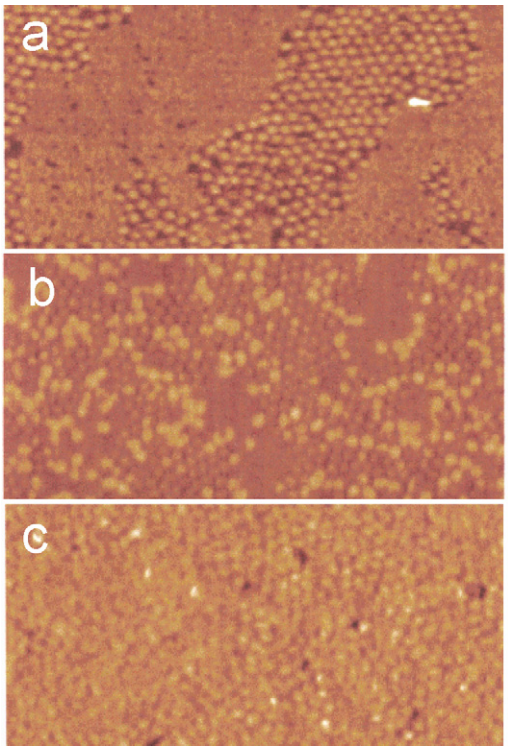

Fig. 6. AFM images (1 μm × 0.5 μm) of mixed DPPE/*F8H16* (1:1.3) Langmuir monolayers transferred onto silicon wafers (Langmuir–Blodgett technique) at (a) 0.5 mN m^{-1}, (b) 10 mN m^{-1}, and (c) 30 mN m^{-1}. The lighter color corresponds to higher level.

Further examples of dynamic pressure-induced vertical phase separation are provided by the reversible ejection/reincorporation of the *F8H2* diblock in monolayers of DPPC when contacted with *F8H2* gas [47], and by the reversible phase separation observed in mixtures of diblock *F8H16* with 10,12-pentacosadiynoic acid (cR. Leblanc et al., Miami University) [48].

4.4. Control of phospholipid film phase behavior

Fluorocarbons and *F*-amphiphiles can interfere with phospholipid films and membranes and drastically modify their phase behavior and other properties. Control of such behavior can sometimes be achieved by simple contact with an *F*C gas. We thus found that *F*C gases (e.g. C_6F_{14}, C_8F_{18}, $C_8F_{17}C_2H_5$, $C_8F_{17}Br$), when added to the atmosphere of air or nitrogen above a monolayer of DPPC, could completely *inhibit* the transition of the monolayer from the liquid expanded (LE) to the liquid condensed (LC) phase that normally occurs when this monolayer is compressed, and thus prevent the formation of semi-crystalline domains [49,50]. Moreover, complete dissolution of LC domains already formed can be achieved by simple contact with an *F*C gas-containing atmosphere (Fig. 7).

Information about the mixing behavior of diverse *F*-surfactants with phospholipids was gathered as background information for the development of pulmonary drug delivery systems and lung surfactant substitutes (collaboration with O. Shibata et al., Fukuoka University). The single-chain semi-fluorinated *F8H11*DMP surfactant **7** was also found to favor dissolution of the ordered LC domains of DPPC [51]. A mixed monolayer was formed when a water-in-*F*-octyl bromide microemulsion formulated with this surfactant was spread on a monolayer of DPPC [52]. Miscibility within mixed Langmuir monolayers of DPPC and (*F*-octyl)pentanol

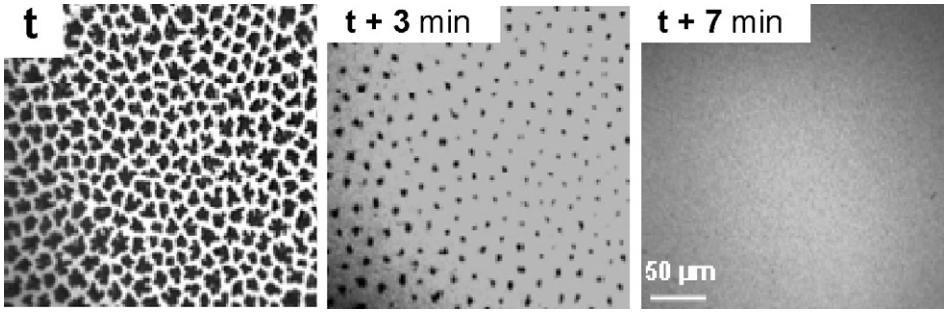

Fig. 7. Fluorescence microscopy images of a monolayer of DPPC compressed at 10 mN m^{-1} under N_2; at time t_0, the nitrogen atmosphere is saturated with *F*-octyl bromide gas, causing the dark semi-crystalline LC phase domains to disappear rapidly; after 7 min, the DPPC monolayer is completely fluidized [50].

(*F8H5*OH) or *F8H5*PC, and the absence of LC domains of DPPC, were demonstrated on the micrometer scale [16]. However, partial phase separation was seen on the nanometer scale and triskelion-shaped domains were observed in the case of the *F*-alkylated alcohol [51]. (*F*-octyl)undecanol (*F8H11*OH) was found to enhance the effectiveness of a pulmonary surfactant model preparation containing the Hel peptide in terms of integrated hysteresis area preservation and maximum reachable surface pressure [17].

4.5. Fluorinated vesicles: nanocompartmented nanoreactors for intrabilayer polymerization

A unique feature of *F*-vesicles is the presence within their membrane of a highly hydrophobic fluorinated central core made of segregated *F*-chains (Scheme 3). This organization creates nanometer size *compartments*, the added central *F*-sub-layer being flanked by two *H*-sub-layers. It also confers to *F*-vesicles specific properties different from those of related *H*-vesicles, including higher stability (e.g. obtaining of heat sterilizable vesicles from single-chain *F*-amphiphiles) [53,54], lower membrane permeability, slower Ca^{++}-induced vesicle fusion [55], and modified behavior in vivo or in biological media [56,57].

F-vesicles made from *F*-alkylated phospholipids of type **4** have *H*-sub-layers that are lipophilic and non-expendable. We showed that the latter can serve as nanoreactors for confined polymerization reactions. Polymerization of hydrophobic monomers (e.g. isodecylacrylate (ISODAC), styrene) is indeed drastically different when performed in *F*-vesicles as compared to standard *H*-vesicles. In the latter case, radical-initiated thermal polymerization of ISODAC yields the previously observed composite "parachute" structure made of a bead of phase-separated polymer attached to the vesicle [58,59]. On the contrary, intrabilayer polymerization in the *F*-vesicles yields capsules [60]. Cryo-TEM images demonstrate homogenous distribution of the polymer within the bilayer, confirming that the *F*-vesicles, by providing confinement in their non-expandable *H*-sub-layers, prevent phase separation of the growing polymer chain.

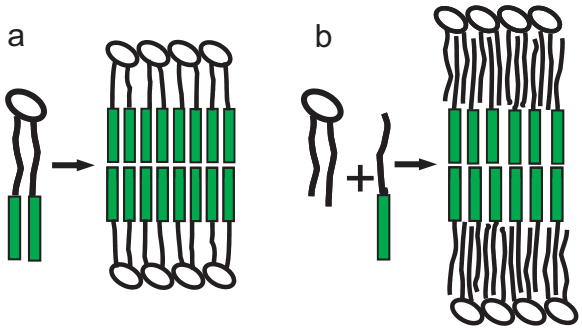

Scheme 4. Two different approaches to *F*-vesicles. Bilayer membranes made of (a) a double chain *F*-phospholipid analogue of a standard phospholipid (e.g. **4**), and (b) a combination of *FnHm* diblock **1** with a phospholipid.

4.6. Structure of the composite F-vesicles combining standard phospholipids and F-alkyl/H-alkyl diblocks

In the *F*-vesicles built by combining standard phospholipids with *FnHm* diblocks, the *Fn* chains avoid contact with both the external aqueous medium and the fatty chains of the lipids by segregating at the centre of the bilayer membrane (Scheme 4). Thereby, a fluorinated core is again expected to form within the membrane. We established that this is indeed the case. The opaque *F*-core can be seen on the cryo-TEM images of unilamellar vesicles of dioleylphosphatidylcholine (DOPC) reinforced by an equimolar amount of *F6H10* (Fig. 8) [61]. Increased vesicle stability is again provided by the strong hydrophobic interactions of the organized *F*-chains core. However, the absence of covalent binding between

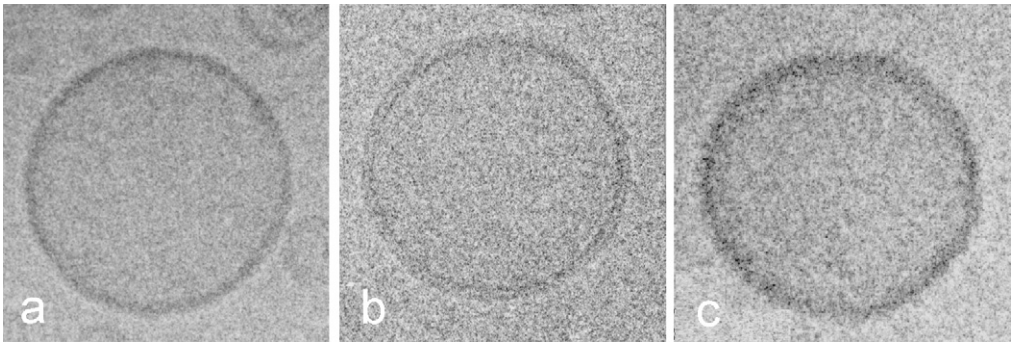

Fig. 8. Cryo-TEM images of vesicles in dispersions of (a) DOPC/*F6H10* (1:1), (b) DOPC alone, and (c) *F*-GPC. The *F*-SUVs seen in (a) and (c) are characterized by a thick dark circle due to the strongly diffracting centrally located *F*-chains, which obscures the two *HC* sub-layers typical of phospholipid bilayers [61].

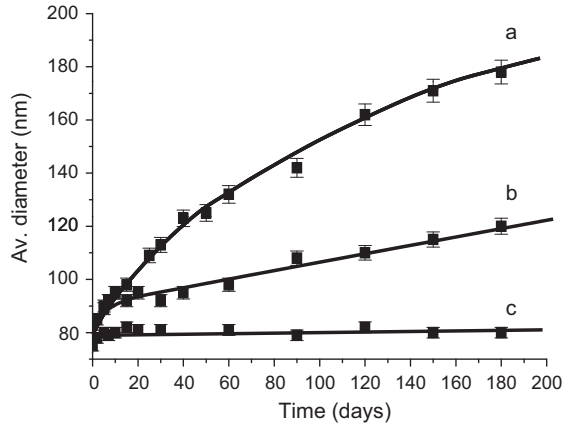

Fig. 9. The increase in size over time (25 °C) of the droplets in an emulsion of $C_8F_{17}Br$ (70% w/v) (a) is very effectively repressed by complementing the phospholipid emulsifier (4% w/v) by an equimolar amount of *F*6*H*10 diblock (c); this stabilizing effect is much more effective than that obtained by the addition of $C_{10}F_{21}Br$ that operates by reducing dispersed phase solubility (b).

the diblocks and lipids make the *H*-sub-layers expandable, and the outcome of intra-bilayer polymerization is not different from that seen with standard non-fluorinated vesicles.

DSC shows significant broadening of the peak corresponding to the gel/fluid phase transition temperature of vesicles of dimyristoylphosphatidylcholine (DMPC) when *F*6*H*10 is incorporated in the formulation, indicating insertion of the diblocks' *H*-moiety among the fatty chains of DMPC. The *F*-moiety of *F*6*H*10 displays a transition at 25 °C when engaged in the bilayer (while this compound is normally liquid at this temperature) indicating that the *F*-moieties form an organized sub-layer within the phospholipids bilayer [61]. SAXS experiments further support the intrabilayer location of the diblock and establish that the *F*-segments are not interdigitated in the central *F*-core.

4.7. FnHm diblock-stabilized fluorocarbon-in-water emulsions—mechanism of stabilization—FnHm diblocks as co-surfactants

Highly effective stabilization of *F*C-in-water emulsions had been obtained by supplementing the phospholipids used as emulsifier by an equimolar amount of an appropriate *FnHm* diblock (Fig. 9). The mechanism of this stabilization has long been controversial. One hypothesis was that the added diblock, by reducing the solubility of the dispersed *F*C phase in the aqueous phase, would reduce the rate of molecular diffusion that is responsible for droplet size increase over time in these emulsions. Our hypothesis was that the diblock, due to its amphiphilic character, is directly involved with the film of phospholipids and modifies its characteristics, including its interfacial tension, and thereby slows down molecular diffusion.

A set of experimental evidence supports the second hypothesis. For example, the amount of phospholipids adsorbed at a *F*C/water interface increases significantly upon addition of the diblock; maximum effect is reached for an equimolar diblock/phospholipid ratio. Diblock *F*6*H*10 dramatically *reduces the tension* of solutions of phospholipids at the *F*C/water interface. Also highly demonstrative of a direct phospholipid/diblock interaction in the interfacial film is the finding that emulsion stabilization (or destabilization) depends sharply on *FnHm* diblock, and more particularly on the length of the *Hm* block relative to that of the phospholipid's fatty chains [62]. The surfactant properties of *FnHm* diblocks are further demonstrated by their capacity to produce and stabilize emulsions of *H*Cs in *F*Cs [1].

4.8. Fluorocarbon-stabilized soft-shell microbubbles

Microbubbles (MBs) are being investigated by SOFFT for several reasons: basic understanding of bubble formation and stability in relation with wall components and inner gas composition; engineering of more stable, better controlled bubble populations, tailor-made for diagnostic imaging, oxygen delivery, ultrasound-triggered drug delivery, etc.

4.8.1. Small bubbles that are more stable than larger ones! Breaking a dogma

Text books concur to state that, because of Laplace pressure ($p = 2\gamma/r$, where γ is the bubble's superficial tension and r its radius), small bubbles will dissolve faster than larger ones made from the same components. Yet, we could reproducibly prepare narrow populations of small microbubbles ($r \approx 1.5$ μm) that have very significantly longer half-lives than larger ones ($r \approx 5.5$ μm) (Fig. 10) [63]. In both cases, the bubble wall consisted of DMPC and the filing gas of nitrogen saturated with *F*-hexane as an osmotic stabilizing agent. This surprising result was traced to an unexpected *co-surfactant* role played by *F*-hexane, in spite of the absence of any obvious amphiphilic character [64].

The co-surfactant effect of *F*-hexane is illustrated by the fact that addition of this *F*C to the air phase causes a significant lowering of the air/water interfacial tension of an aqueous dispersion of DPPC [63]. Also, the rate of adsorption of the phospholipid at the interface is considerably accelerated. Both effects are concentration-dependent. Since the partial pressure of

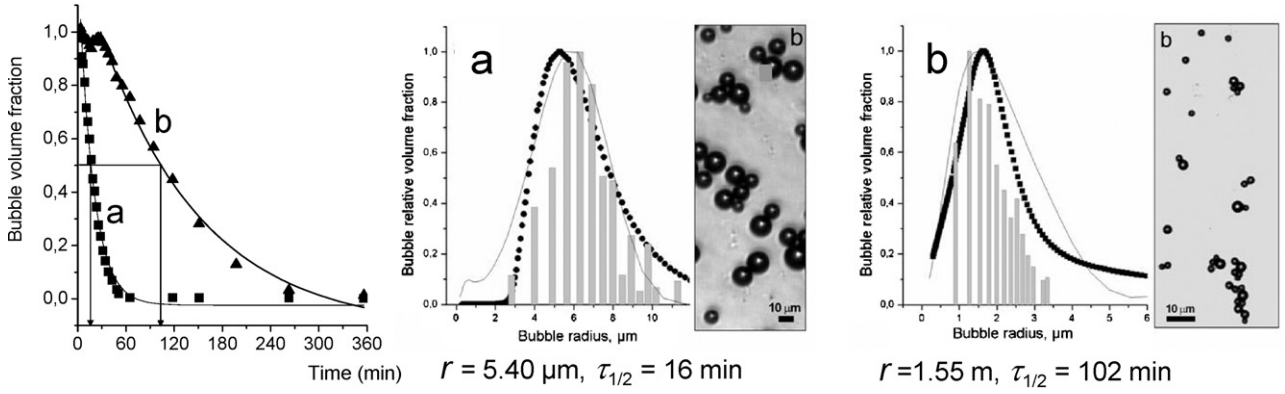

Fig. 10. Microbubbles with a shell of DMPC, osmotically stabilized with *F*-hexane. Acoustical determinations show that the half-life of the small bubbles (b, *r* 1.5 μm) is substantially longer (102 min) than that of the larger bubbles (a, *r* 5.4 μm, 16 min); particle size histograms and optical micrographs are shown for the two bubble populations [63].

F-hexane is higher in the smaller bubbles, its co-surfactant effect should, therefore, be larger. Consequently the tension lowering effect should be larger for the smaller bubbles, resulting in a lowering of Laplace pressure and to stabilization of the smaller bubbles relative to the larger ones. The phenomenon was observed for a series of phospholipids.

4.8.2. Synergy between a fluorinated wall component and a fluorocarbon inner gas

The half-live of microbubbles in an ultrasound wave field can be increased by an order of magnitude using di(*F*6*H*6)GPC **4** instead of DMPC as wall component, provided an *F*C gas is present inside the bubble [65]. Moreover, *F*-surfactants allowed us to produce monomodal bubble populations in a large, 2–20 μm average size range, depending on *F*-surfactant structure [33].

4.9. Decorated microbubbles

Preliminary confocal microscopy studies of our recently produced Fe_3O_4NP-*deco*MBs (see Section 2.3.4.) allowed imaging of collections of microbubbles, confirmed the presence of NP aggregates on their surface, demonstrated that the NPs are mobile in the interfacial film, and that the hybrid micron-size objects are stable enough for investigation (collaboration with J.-Y. Bigot et al., IPCMS Strasbourg). When submitted to a magnetic field the Fe_3O_4NP-*deco*MBs align themselves along the direction of the field (Scheme 3) [66].

5. Assessing the potential of fluorinated self-assemblies in biomedical and materials sciences

Exploratory investigations aiming at developing new aids for diagnosis and therapy include lung surfactant substitutes; use of *F*C emulsions for tissue and pancreatic islet preservation, for cell adhesion control, as oxygen carriers, contrast agents, and tools for biomedical research; and use of microbubbles as multimodal contrast agents for diagnosis, and for oxygen delivery [67,68]. Assessment of potential applications of our self-assembled constructs in materials science is being increasingly pursued. These projects are led in collaboration with specialists in the relevant fields.

5.1. Lung surfactant replacement preparations

Some serious health conditions that affect neonates and infants as well as adults require administration of surfactant substitutes. DPPC, the major component of natural lung surfactant, cannot play this role when alone, because it forms semi-crystalline LC domains on the alveolar surface upon compression (i.e. during expiration) that hinder its re-spreading upon expansion (inspiration). We found that contact with *F*C gases suppresses the transition of DPPC monolayers from the LE to the LC phase upon compression (Section 3.4) [47,49,50]. Combining DPPC and *F*C administration, as in the form of an emulsion, provides a means of restoring lung surfactant functionality. Experimentation on premature rabbits that lack adequate surfactant production demonstrated indeed a rapid and significant increase in alveolar tidal volume following pulmonary administration of an *F*C emulsion, indicating effective surfactant activity (collaboration with Boerhinger-Ingelheim, Germany).

Furthermore, we showed that monolayers of DPPC, when brought in contact with an *F*C gas, are significantly less sensitive to the deleterious effect of albumin [69]. This protecting effect is interesting since the acute respiratory distress syndrome (ARDS) is often accompanied by the presence of albumin and other proteins in the alveoli where they have a damaging delipiding effect.

5.2. Control of the adhesion properties of cultured cells—promotion of insulin secretion

In the course of collaborative work on a bioartificial pancreas, for which efficient oxygenation of Langerhans cells is a challenge, we observed that diblock-stabilized *F*C emulsions could prevent the adhesion of certain β-cell lines to cell culture plastic Petri boxes, and promote the formation of pseudo-islets capable of insulin secretion (Fig. 11; collaboration with S. Sigrist et al., Centre Européen d'Etude du Diabète, Strasbourg) [70].

5.3. Oxygen delivery

The oxygen delivery efficacy of the *FnHm* diblock-stabilized *F*C emulsions has been demonstrated for isolated tissues, cells and organ preservation (collaboration with G. Deby et al. Centre de Biochimie de l'Oxygène, Université de Liège) [71,72]. These emulsions were also beneficial to Langerhans islets, which are

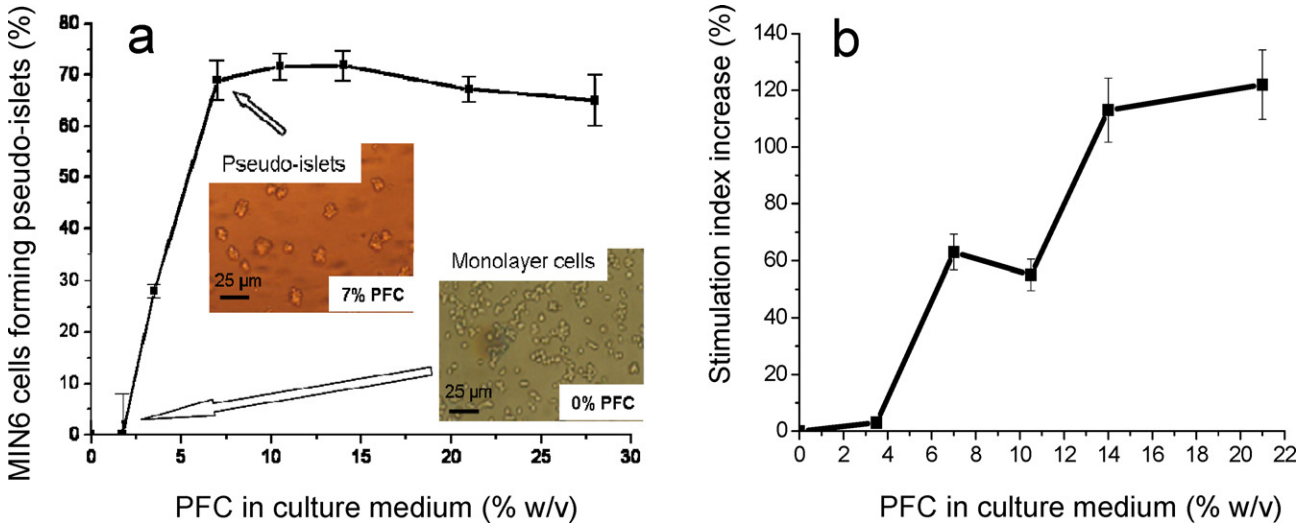

Fig. 11. (a) Contact with an *F*C emulsion causes MIN6 cells to detach from the Petri dish and to aggregate into pseudo-islets; (b) glucose stimulation causes these pseudo-islets to produce insulin [70].

particularly prone to necrosis [73]. Rabbits were resuscitated after severe hemorrhagic shock by treatment with such an emulsion [74]. The emulsion increased oxygen delivery to the skeletal muscle. No measurable deleterious effects were noted (collaboration with P. Menu et al., Université de Nancy). The unsavory issue of doping was also considered, for which a GC/MS assay for *F*Cs in blood and the expired air was established (collaboration with M. Audran et al., Université de Montpellier, J. de Ceaurriz, Châtenay-Malabry) [75,76].

5.4. FC-in-water emulsions as research tool—brain imaging for neurosciences

Near-total exchange of the blood of rats by a diblock-stabilized *F*C emulsion greatly improved two-photon laser-scanning microscopy of the brain cortex by preventing light scattering by blood cells and absorption by hemoglobin [77]. This procedure allowed in vivo imaging with sub-cellular resolution of complete populations of neurons and astrocytes of the neocortex, including those normally obscured by the blood vessels that irrigate the brain (Fig. 12). The normal physiological parameters (pCO_2, pH, arterial blood pressure) were not affected by the exchange transfusion by the *F*C emulsion, but for O_2 pressure, which increased significantly. Neuronal integrity was preserved (collaboration with B. Weber et al., ETH, Zurich).

5.5. Reverse water-in-FC emulsions for pulmonary drug delivery

Reverse water-in-*F*C emulsions and microemulsions are promising vehicles for pulmonary delivery of genetic material, anticancer and other agents. The safety of *F*Cs when infused in the lung had been demonstrated [78,79]. The *F*C that now carries dispersed drug-loaded water droplets ensures rapid and homogenous dispersion of the drug in the lung.

The *F*8*H*11DMP surfactant **7** that provided the most stable emulsions was selected and tested for biocompatibility on human pulmonary cells (collaboration with Th. Vandamme, Fac. Pharmacie, Université de Strasbourg) [80]. Tolerance increased with total hydrophobic chain length and *Fn*/*Hm* ratio, and was higher than for the *H*C analogues. Biocompatibility was confirmed by confocal microscopy examination of fibroblasts. The emulsions were well tolerated in mice and delayed the delivery of insulin [81]. Water-in-*F*C emulsions formulated as aerosols propelled by hydrofluoroalkanes allowed homogenous and reproducible delivery of caffeine [82].

5.6. Emulsions and microemulsions as research tools—controlled confinement

Reverse water-in-*F*C microemulsions provide ideal confinement tools in which the test molecule is enclosed in a small, controllable size aqueous space, and isolated from external influences by the surrounding hydrophobic and lipophobic *F*C phase. Using a water-in-*F*-octyl bromide microemulsion emulsified with *F*8*H*11DMP, infrared spectroscopy determined that confinement size has a strong influence on the dynamics of confined water (collaboration with A. Gerschel, LCP, P. Roy, LURE, Orsay) [83]. The same confinement tool should be applicable to biomolecules (e.g. proteins, nucleic acids, viruses), whose functional properties are known to depend on both their structure and their dynamics. Reverse microemulsions should allow limitation of the hydration of biomolecules, while preserving their functional configuration.

5.7. Microbubbles as sound reflectors for diagnosis

Enhanced bubble stability, and control of bubble/sound interactions and harmonic wave generation, should allow expansion of the field of contrast imaging (e.g. to deep set tumors), as well as of ultra-sound triggered clot-breaking or focalized drug delivery. An ongoing collaboration (G. Pourroy et al., IPCMS, Strasbourg) assembles and investigates microbubbles decorated with magnetic particles. These constructs should constitute dual contrast agents for both ultrasound and magnetic resonance imaging [66].

5.8. Decorated microbubbles for multi-scale devices

Controlled engineering of flexible microbubbles decorated with nanoparticules is important for the development of new multiscale devices for high performance photonics, electronics information, optics and magneto-optics. Control of NPs' size, number and interdistances at the surface of the MB spheres is a key issue. Therefore, we are building MBs that are coated with a *fluid* film of

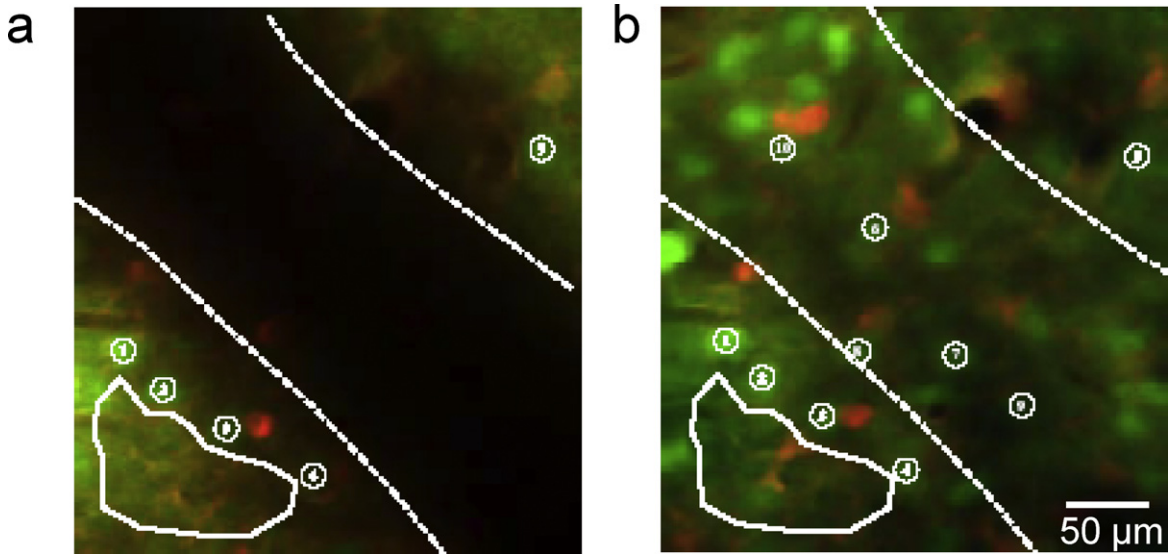

Fig. 12. Two-photon microscopy images of rat brain cortex (180 μm deep), (a) in the presence of red cells and hemoglobin, the blood vessel (doted line) absorbs and diffuses light, making observation of brain cells impossible; (b) after exchange-transfusion of the blood of the animal with an *F*C emulsion, the vessel becomes transparent, and observation of astrocytes (red) and neurons (green) is possible [77].

amphiphiles on which NPs are grafted with controlled density, and maintain flexible and mobile interactions (collaboration with G. Pourroy et al., IPCMS). Two types of elements of markedly different sizes, the NPs (a few nm) and MBs (several hundred to several μm) are associated in these modular superstructures. The magnetic interactions of Fe_3O_4NP-decoMBs will be investigated on three levels: within the NPs, between NPs on a given MB, and between magnetic MBs [66].

5.9. Surface patterning

The sturdy micelle-patterned solid surfaces obtained by deposition of *FnHm* diblocks **1** and di(*FnHm*) tetrablocks **14** could serve as nano-masks in the bottom-up approach to information storage and processing devices, photovoltaic devices, and for catalysis. Independent work has indeed demonstrated formation of regular hexagonal arrays of metallic nano-dots on a solid substrate [84]. Using gold, such metal networks were able to catalyze oxidation of CO into CO_2. Other Langmuir–Blodgett films have been successfully used as templates to produce thin patterned SiO_2 films [85]. Arrays of self-assembled hemimicelles could also be useful for exploring the interactions of cultured living cells with patterned surfaces.

6. Conclusion

Our knowledge of fluorinated soft matter has significantly advanced during the past decade. Yet, the powerful capacity of *F*-chains to build, organize and stabilize self-assembled systems and nanomaterials, together with their specific properties, still remains underexploited. New perspectives include design of therapeutic and diagnosis contrast agents, chemo- and biosensors, abiotic protein and nucleic acid pairing, and hybrid inorganic/organic *F*-SAMS with potential in electronics and photovoltaics.

Research topics

The SOFFT (Systèmes Organisés Fluorés à Finalités Thérapeutiques) (Self-Organized Fluorinated Systems for Therapeutics) team was founded in 2000 at the Institut Charles Sadron (ICS) of the Centre National de la Recherche Scientifique (CNRS) in Strasbourg. Our main research focus is on the design, engineering and investigation of functional self-assembled micro- and nanometer-size fluorinated molecular systems, films and membranes. We aim at building complex, multicompartmented, multiscale functional objects, understanding the fundamentals that determine their self-assembly, structure and properties, and explore their potential applications, primarily in the biomedical field, and increasingly also for materials science. Therefore, we take advantage of the specific properties of perfluoroalkylated chains and, in particular, of their extreme hydrophobic (and lipophobic) character, surface activity, and strong self-assembling and organizing capacity; we also synthesize the required perfluoroalkylated components (see Scheme 1).

Since its foundation, the team benefited from the contributions of about 15 people, mostly Ph.D. students and Post-Docs, whose names appear as authors of the primary publications listed in the references. Our research is supported by the CNRS and the Centre International de Recherche aux Frontières de la Chimie (FRC) of the Université de Strasbourg, and by contracts and grants from the French Agence Nationale pour la Recherche (ANR) and European Commission (7th Framework NMP program, Nanotechnology and nanosciences, multifunctional Materials and new Production processes). The team benefits from strong collaborations with Colleagues from the physics and biomedical communities. Its specific equipment includes labs for synthesis and physical chemistry, as well as a Class 100.000 clean room with high shear emulsification devices, and acoustical methods for investigation of microbubbles. It also has access to the heavier equipment of the ICS and from the nearby Institut de Physique et Chimie des Matériaux de Strasbourg (IPCMS).

Acknowledgements

Grateful thanks to my Co-workers and Colleagues of the SOFFT team; the ICS, CNRS, Université de Strasbourg, FRC, GIS-Fluor, ANR, European Commission, for support.

References

[1] M.P. Krafft, J.G. Riess, Chem. Rev. 109 (2009) 1714–1792.
[2] J.N. Israelachvili, D.J. Mitchell, B.W. Ninham, Biochim. Biophys. Acta 470 (1977) 185–201.
[3] M.P. Turberg, J.E. Brady, J. Am. Chem. Soc. 110 (1988) 7797–7801.
[4] M. Sanchez-Dominguez, N. Benoit, M.P. Krafft, Tetrahedron 64 (2008) 522–528.
[5] C. de Gracia Lux, M.P. Krafft, Chem. Eur. J. 16 (2010) 11539–11542.
[6] V.M. Sadtler, F. Jeanneaux, M.P. Krafft, J. Rabai, J.G. Riess, New J. Chem. 22 (1998) 609–613.
[7] V.M. Sadtler, F. Giulieri, M.P. Krafft, J.G. Riess, Chem. Eur. J. 10 (1998) 1952–1956.
[8] Z. Szlávik, A. Csampai, M.P. Krafft, J.G. Riess, J. Rábai, Tetrahedron Lett. 38 (1997) 8757–8760.
[9] M.P. Krafft, F. Jeanneaux, M. Le Blanc, J.G. Riess, Anal. Chem. 60 (1988) 1969–1972.
[10] J.A. Gladysz, D.P. Curran, I. Horváth, Handbook of Fluorous Chemistry, Wiley-VCH, Weinheim, 2004.
[11] M.P. Krafft, J.G. Riess, Biochimie 80 (1998) 489–514.
[12] J.G. Riess, M.P. Krafft, Mater. Res. Soc. Bull. 24 (1999) 42–48.
[13] M.P. Krafft, J.G. Riess, J. Polym. Sci. Part A: Polym. Chem. 45 (2007) 1185–1198.
[14] O. Shibata, M.P. Krafft, Langmuir 16 (2000) 10281–10286.
[15] H. Nakahara, S. Nakamura, H. Kawasaki, O. Shibata, Colloids Surf. B 41 (2005) 285–298.
[16] S. Nakamura, H. Nakahara, M.P. Krafft, O. Shibata, Langmuir 23 (2007) 12634–12644.
[17] H. Nakahara, S. Lee, M.P. Krafft, O. Shibata, Langmuir 26 (2010) 18256–18265.
[18] F. Guillod, J. Greiner, J.G. Riess, Carbohydr. Res. 261 (1994) 37–55.
[19] A. Gonzàlez-Pérez, M. Schmutz, G. Waton, M.J. Romero, M.P. Krafft, J. Am. Chem. Soc. 129 (2007) 756–757.
[20] M. Dubois, B. Demé, T. Gulik-Krywicki, J.-C. Dedieu, C. Vautrin, S. Désert, E. Perez, T. Zemb, Nature 411 (2001) 672–675.
[21] M. Dubois, V. Lizunov, A. Meister, T. Gulik-Krywicki, J.-M. Verbavatz, E. Perez, J. Zimmerberg, T. Zemb, Proc. Natl. Acad. Sci. U.S.A. 101 (2004) 15082–15087.
[22] F. Giulieri, M.P. Krafft, J.G. Riess, Angew. Chem. Int. Ed. Engl. 33 (1994) 1514–1515.
[23] F. Giulieri, M.P. Krafft, J. Colloid Interface Sci. 258 (2003) 335–344.
[24] F. Giulieri, F. Guillod, J. Greiner, M.P. Krafft, J.G. Riess, Chem. Eur. J. 2 (1996) 1335–1339.
[25] T. Imae, K. Funayama, M.P. Krafft, F. Giulieri, T. Tada, M. Matsumoto, J. Colloid Interface Sci. 212 (1999) 330–337.
[26] T. Imae, M.P. Krafft, F. Giulieri, T. Matsumoto, T. Tada, Prog. Colloid Polym. Sci. 106 (1997) 52–56.
[27] F. Giulieri, M.P. Krafft, Thin Solid Films 284/285 (1996) 195–199.
[28] M.P. Krafft, F. Giulieri, J.G. Riess, Phosphorus, Sulfur, Silicon 111 (1996) 76.
[29] C. Cornélus, M.P. Krafft, J.G. Riess, Artif. Cells Blood Subst. Immob. Biotechnol. 22 (1994) 1183–1191.
[30] V.M. Sadtler, M.P. Krafft, J.G. Riess, Angew. Chem. Int. Ed. Engl. 35 (1996) 1976–1978.
[31] H.M. Courrier, T.F. Vandamme, M.P. Krafft, Colloids Surf. A: Physicochem. Eng. Aspects 244 (2004) 141–148.
[32] M.P. Krafft, J.G. Riess, Angew. Chem. Int. Ed. Engl. 33 (1994) 1100–1101.
[33] S. Rossi, G. Waton, M.P. Krafft, Langmuir 26 (2010) 1649–1655.
[34] G.L. Gaines, Langmuir 7 (1991) 3054–3056.
[35] Z. Huang, A.A. Acero, N. Lei, S.A. Rice, Z. Zhang, M.L. Schlossman, J. Chem. Soc. Faraday Trans. 92 (1996) 545–552.
[36] M.P. Krafft, M. Goldmann, Curr. Opin. Colloid Interface Sci. 8 (2003) 243–250.
[37] M. Maaloum, P. Muller, M.P. Krafft, Angew. Chem. Int. Ed. 41 (2002) 4331–4334.
[38] G. Zhang, M. Maaloum, P. Muller, N. Benoit, M.P. Krafft, Phys. Chem. Chem. Phys. 6 (2004) 1566–1569.
[39] G.-F. Zhang, P. Marie, M. Maaloum, P. Muller, N. Benoit, M.P. Krafft, J. Am. Chem. Soc. 127 (2005) 10412–10419.
[40] A. Mourran, B. Tartsch, M.O. Gallyamov, S. Magonov, D. Lambreva, B.I. Ostrovskii, I.P. Dolbnya, W.H. de Jeu, M. Moeller, Langmuir 21 (2005) 2308–2316.
[41] M.O. Gallyamov, A. Mourran, B. Tartsch, R.A. Vinokur, L.N. Nikitin, A.R. Khokhlov, K. Schaumburg, M. Möller, Phys. Chem. Chem. Phys. 8 (2006) 2642–2649.
[42] P. Fontaine, M. Goldmann, P. Muller, M.-C. Fauré, O. Konovalov, M.P. Krafft, J. Am. Chem. Soc. 127 (2005) 512–513.
[43] A. Gonzàlez-Pérez, C. Contal, M.P. Krafft, Soft Matter 3 (2007) 191–193.
[44] A.N. Semenov, A. Gonzàlez-Pérez, M.P. Krafft, J.-F. Legrand, Langmuir 22 (2006) 8703–8717.
[45] C. de Gracia Lux, J.-L. Gallani, G. Waton, M.P. Krafft, Chem. Eur. J. 16 (2010) 7188.
[46] M. Maaloum, P. Muller, M.P. Krafft, Langmuir 20 (2004) 2261–2264.

[47] F. Gerber, T.F. Vandamme, M.P. Krafft, C.R. Acad. Sci. (Chimie) 12 (2009) 180–187.
[48] S. Wang, R. Lunn, M.P. Krafft, R.M. Leblanc, Langmuir 16 (2000) 2882–2886.
[49] F. Gerber, M.P. Krafft, T.F. Vandamme, M. Goldmann, P. Fontaine, Angew. Chem. Int. Ed. 44 (2005) 2749–2752.
[50] F. Gerber, M.P. Krafft, T.F. Vandamme, M. Goldmann, P. Fontaine, Biophys. J. 90 (2006) 3184–3192.
[51] T. Hiranita, S. Nakamura, M. Kawachi, H.M. Courrier, T.F. Vandamme, M.P. Krafft, O. Shibata, J. Colloid Interface Sci. 265 (2003) 83–92.
[52] H.M. Courrier, T.F. Vandamme, M.P. Krafft, S. Nakamura, O. Shibata, Colloids Surf. A: Physicochem. Eng. Aspects 215 (2003) 33–41.
[53] M.P. Krafft, F. Giulieri, J.G. Riess, Angew. Chem. Int. Ed. Engl. 32 (1993) 741–743.
[54] F. Giulieri, M.P. Krafft, Colloids Surf. 84 (1994) 121–127.
[55] Y. Ferro, M.P. Krafft, Biochim. Biophys. Acta 1581 (2002) 11–20.
[56] J.G. Riess, J. Drug Target. 2 (1994) 455–468.
[57] J.G. Riess, M.P. Krafft, Chem. Phys. Lipids 75 (1995) 1–14.
[58] M. Jung, D.H.W. Hubert, P.H.H. Bomans, P.M. Frederik, J. Meuldijk, A.M. van Herk, H. Fischer, A.L. German, Langmuir 13 (1997) 6877–6880.
[59] H.-P. Hentze, E.W. Kaler, Curr. Opin. Colloid Interface Sci. 8 (2003) 164–178.
[60] M.P. Krafft, L. Schieldknecht, P. Marie, F. Giulieri, M. Schmutz, N. Poulain, E. Nakache, Langmuir 17 (2001) 2872–2877.
[61] M. Schmutz, B. Michels, P. Marie, M.P. Krafft, Langmuir 19 (2003) 4889–4894.
[62] S. Marie Bertilla, J.-L. Thomas, P. Marie, M.P. Krafft, Langmuir 20 (2004) 3920–3924.
[63] S. Rossi, G. Waton, M.P. Krafft, ChemPhysChem 9 (2008) 1982–1985.
[64] P.N. Nguyen, G. Waton, T.F. Vandamme, M.P. Krafft, 16th Europ. Conf. Fluorine Chem., Ljubljana, Slovenia, 2010.
[65] F. Gerber, M.P. Krafft, G. Waton, T.F. Vandamme, New J. Chem. 30 (2006) 524–527.
[66] G. Nikolova, P.N. Nguyen, J. Ma, G. Waton, N. Benoit, M.P. Krafft, L.T. Phuoc, G. Pourroy, Conference on Hybrid Materials Strasbourg, March 2011.
[67] J.G. Riess, M.P. Krafft, Artif. Cells Blood Subst. Immob. Biotechnol. 25 (1997) 43–52.
[68] M.P. Krafft, J.G. Riess, in: A. Tressaud, G. Haufe (Eds.), Advances in Fluorine Science – Fluorine and Health. Molecular Imaging, Biomedical Materials and Pharmaceuticals, Elsevier, Amsterdam, 2008, pp. 447–486 (Chapter 11).
[69] F. Gerber, M.P. Krafft, T.F. Vandamme, Biochim. Biophys. Acta – Biomembranes 1768 (2007) 490–494.
[70] M. Sanchez-Dominguez, M.P. Krafft, E. Maillard, S. Siegrist, A. Belcourt, ChemBioChem 7 (2006) 1160–1163.
[71] A. DeRoover, M.P. Krafft, G. Deby-Dupont, J.G. Riess, N. Jacquet, M. Lamy, M. Meurisse, M. D'Silva, Artif. Cells Blood Subst. Immob. Biotechnol. 29 (2001) 225–234.
[72] J.G. Riess, Chem. Rev. 101 (2001) 2797–2920.
[73] E. Maillard, M. Sanchez-Dominguez, C. Kleiss, A. Langlois, M.C. Sencier, C. Vohouhe, W. Beitigier, M.P. Krafft, M. Pinget, A. Belcourt, S. Sigrist, Transplantation Proceedings, Elsevier, New York, 2008, pp. 372–374.
[74] S. Audonnet-Blaise, M.P. Krafft, Y. Smani, P.-M. Mertes, P.-Y. Marie, P. Labrude, D. Longrois, P. Menu, Resuscitation 70 (2006) 124–132.
[75] M. Audran, M.P. Krafft, J. De Ceaurriz, J.-C. Maturin, M.-T. Sicart, B. Marion, G. Bougard, F. Bressole, J. Chromatogr. B 745 (2000) 333–343.
[76] J.-C. Mathurin, J. de Ceaurriz, M. Audran, M.P. Krafft, Biomed. Chromatogr. 15 (2001) 443–451.
[77] F. Haiss, R. Jolivet, M.T. Wyss, J. Reichold, N.B. Braham, F. Scheffold, M.P. Krafft, B. Weber, J. Physiol. 587 (2009) 3153–3158.
[78] C.L. Leach, J.S. Greenspan, D. Rubenstein, T.H. Shaffer, M.R. Wolfson, J.C. Jackson, R. DeLemos, B.P. Fuhrman, New Engl. J. Med. 335 (1996) 761–766.
[79] M.R. Wolfson, T.H. Shaffer, Paediatr. Respir. Rev. 6 (2005) 117–127.
[80] H.M. Courrier, M.P. Krafft, N. Butz, C. Porté, N. Frossard, A. Rémy-Kristensen, Y. Mély, F. Pons, T.F. Vandamme, Biomaterials 24 (2003) 689–696.
[81] H.M. Courrier, F. Pons, J.M. Lessinger, N. Frossard, M.P. Krafft, T.F. Vandamme, Int. J. Pharm. 282 (2004) 131–140.
[82] N. Butz, C. Porté, H. Courrier, M.P. Krafft, T.F. Vandamme, Int. J. Pharm. 238 (2002) 257–269.
[83] J.-B. Brubach, A. Mermet, A. Filabozzi, A. Gerschel, D. Lairez, M.P. Krafft, P. Roy, J. Phys. Chem. B 105 (2001) 430–435.
[84] E. Charrault, M. He, P. Muller, M. Maaloum, C. Petit, P. Petit, Langmuir 25 (2009) 11285–11288.
[85] S. Kataoka, Y. Takeuchi, A. Endo, Langmuir 26 (2010) 6161–6163.